Spectroscopic Study of Maghemite Nanoparticles Surface-Grafted with DMSA

ARTICLE *in* THE JOURNAL OF PHYSICAL CHEMISTRY A · FEBRUARY 2011

Impact Factor: 2.69 · DOI: 10.1021/jp1109916 · Source: PubMed

THE JOURNAL OF PHYSICAL CHEMISTRY A

ARTICLE

pubs.acs.org/JPCA

Spectroscopic Study of Maghemite Nanoparticles Surface-Grafted with DMSA

Maria A. G. Soler,*[,†] Emilia C. D. Lima,[‡] Eloiza S. Nunes,[‡] Fabio L. R. Silva,[†] Aderbal C. Oliveira,[†] Ricardo B. Azevedo,[§] and Paulo C. Morais[†]

[†]Instituto de Física, Universidade de Brasília, Brasília DF 70910-900, Brazil

[‡]Instituto de Química, Universidade Federal de Goiás, Goiânia GO 74001-970, Brazil

[§]Instituto de Ciências Biologicas, Universidade de Brasília, Brasília DF 70910-900, Brazil

ABSTRACT: Nanosized maghemite (below 10 nm average diameter), surface-functionalized with *meso*-2,3-dimercaptosuccinic acid (DMSA), was investigated with respect to the content of DMSA molecules attached onto its surface and the onset of S−S bridges due to oxidation of neighboring S−H groups. To support our investigation, we introduced the use of photoacoustic spectroscopy to monitor thiol groups (S−H) conjugated with Raman spectroscopy to monitor the disulfide bridges (S−S). The normalized intensity (N_R) of the Raman feature peaking at 500 cm^{-1} was used to probe the S−S bridge whereas the normalized intensity (N_P) of the photoacoustic band-S (0.42−0.65 μm) was used to probe the S−H moiety. The perfect linearity observed in the N_R versus $(1 - N_P)$ plot strongly supports the oxidation process involving neighboring S−H groups as the DMSA surface grafting coefficient increases whereas the approach used in this report allows the evaluation of the [S−H]/[S−S] ratio. The observation of the reduction of the hydrodynamic diameter as the nominal DMSA-grafting increases supports the proposed model picture, in which the intraparticle (interparticle) S−S bridging takes place at higher (lower) DMSA-grafting values.

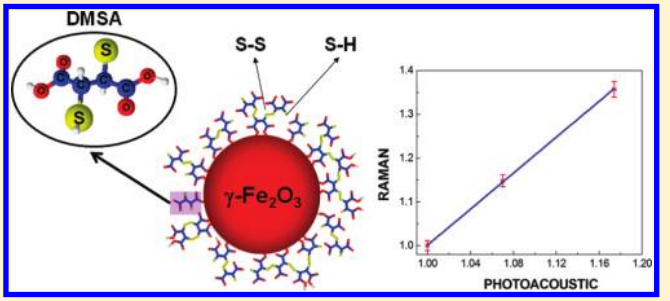

INTRODUCTION

The surface functionalization of bare superparamagnetic iron oxide (SPIO) particles using previously selected molecules is a key point while tailoring these materials for both industrial and medical applications. Commercial insulating oil containing surface-dressed SPIO particles in suspension has been successfully prepared for improvement of transformer's cooling efficiency.[1] High-resolution MRI technology can be realized by magnetically tagging tumor cells using SPIO-based materials.[2,3] Chemotherapeutic agents can be attached to surface-functionalized SPIO particles, thus allowing their site localization (tumor region) via application of magnetic field gradients after injection into the blood circulation and/or nearby the tumor site.[4] Indeed, the use of surface-functionalized SPIO particles as a material platform to fabricate complex magnetic drug delivery systems has attracted considerable interest in recent years.[5−7]

While developing surface-functionalized SPIO-based systems addressed to medical applications, one has to carefully take into account basic aspects, among others the chemical characteristics of the molecular coating layer and the physical properties of the SPIO core. It is worth notice that in many applications the SPIO surface functionalization represents just the intermediate step toward binding bioactive molecules in a latter stage.[8,9] The chemical and the physical characteristics of the end product depend on both the SPIO synthesis route and the protocols used in the surface functionalization.[10] The coating and the core material characteristics not only affect the efficiency of the SPIO-based product while addressed to a particular application but also influence cell internalization, biodistribution, nanotoxicity, metabolization, and clearance parameters.[11]

Among the surface-coatings used nowadays, *meso*-2,3-dimercaptosuccinic acid (DMSA) has been successfully employed in the surface functionalization of SPIO-based materials.[12−16] In addition, DMSA-coating also allows efficient transfer of the functionalized SPIO particles from organic to aqueous phase,[7,17−19] providing improved stability and easy conjugation to bioactive molecules. Biodistribution investigation of DMSA-coated magnetite nanoparticles intravenously injected in mice was conducted using light microscopy and magnetic resonance, revealing enhanced organ specificity to lung, which collects almost all the particles 30 min after the animal's injection.[13] The preferential uptake of DMSA functionalized SPIO particles by lung was confirmed in an extended time window experiment, showing that organ inflammation was actually induced by the treatment.[14]

In nanosized iron-based SPIO particles, DMSA molecules are known to be covalently bonded at iron sites onto the particle's

Received: July 12, 2010
Revised: December 27, 2010
Published: January 25, 2011

surface through the carboxylate terminal while intermolecular disulfide cross-linkages (S−S) among neighboring molecular units are claimed to help stabilize the molecular surface layer.[12] It is worth mentioning, however, that with the exception of this report no experimental evidence for the S−S bridging resulting from neighboring DMSA molecules attached onto the same nanosized particle (which improves colloidal stability) or from DMSA molecules attached onto neighboring nanosized particles (which reduces colloidal stability) has been presented in the literature. The remaining DMSA free S−H groups have been used to attach target-specific biomolecules, as for instance antibodies for labeling cancer cells[17] or for MRI cancer diagnosis.[18] In spite of the key influence of thiol groups in biological events and the importance of the availability of this functional group to attach specific molecules, there is no spectroscopic techniques available in the literature to probe thiol groups attached onto iron oxide surfaces, except via destructive analytical methods. For instance, in the infrared spectroscopy the band absorption of thiol groups is not intense, which makes difficult the thiol detection while in small amounts in surface-functionalized nanoparticles.[20] In contrast, Raman spectroscopy is an excellent tool to detect the thiol group in molecules due to its enhanced Raman scattering. The grafting of the thiol group onto colloidal mesoporous silica was fully characterized by Raman spectroscopy.[21] On the other hand, detection of thiol groups grafted onto iron oxide nanoparticles using Raman spectroscopy is quite difficult due to the strong absorption of the incident light by the dark iron oxide cores, leading to very weak Raman scattering from DMSA molecules adsorbed at the nanoparticle's surface. Moreover, by using a visible laser excitation source, the intense emission band of the iron oxide core hides the thiol characteristic Raman band. With this in mind and aiming to investigate DMSA grafted onto nanosized maghemite, we propose the use of both photoacoustic spectroscopy and Raman spectroscopy to monitor thiol groups (S−H) and the associated disulfide bridges (S−S), the latter resulting from the oxidation of the former. Considering the important role the thiol group plays in biological systems and the huge interest in DMSA-grafted SPIO systems to support biological and medical applications, the aim of this work is to study the DMSA adsorption onto the surface of nanosized maghemite and the possible scenarios for intermolecular disulfide cross-linking among DMSA units as a function of the amount of DMSA used in the surface-coating process. Raman spectroscopy (RS) and photoacoustic spectroscopy (PAS)[22] were selected as analytical tools to systematically and comparatively investigate the DMSA intermolecular disulfide cross-linking while the molecule is used to functionalize SPIO particles. Separately, both spectroscopic techniques have been successfully used in the analysis of microscopic details of molecular layers dressing nanosized particles.[23−27] The comparative analysis carried out in the present study involving RS and PAS improves the understanding of the SPIO dressing layer while provides the basis for quality control of DMSA-functionalized nanosized materials using the photoacoustic (PA) effect.

EXPERIMENTAL SECTION

Chemicals and Materials. All chemicals used in this study were analytical grade and employed without additional purification, purchased from Merck, Synth, or Aldrich. Ultrapure water (18 MΩ × cm resistivity) was provided by the Elga purification system.

Sample Preparation and Description. A DMSA-coated maghemite nanoparticle (DMSA-Mag) was produced and dispersed in aqueous medium according to the procedure previously reported in the literature.[28] Shortly, nanosized magnetite (Fe_3O_4) was synthesized by mixing Fe(II) and Fe(III) aqueous chloride solutions (2:1 molar ratio) with concentrated ammonia solution (25%) under vigorous stirring. The resulting black precipitate consisting of nanosized magnetite was washed several times with water and separated from the supernatant using a permanent magnet. The oxidation of nanosized magnetite to maghemite was performed by dispersing the magnetite sample in boiling solution of 0.35 mol × L^{-1} $Fe(NO_3)_3$ under stirring, for 1 h.[29] The structural properties of the resulting oxidized nanoparticles determine the magnetic properties that can be modified either by changing the magnetite preparation route[30] or by using different oxidation processes.[1] The nanoparticulated sample was then washed with 2.0 mol × L^{-1} HNO_3 aqueous solution and separated from the supernatant using a permanent magnet. The reddish sediment, containing the nanosized surface-uncoated maghemite sample (labeled pMag), was dispersed in deionized water and the dispersion was shaken for 12 h. The maghemite dispersion was further centrifuged at 5000 rpm for 5 min for separation of nonsuspended material. This purified maghemite-based dispersion (20 mL) was then treated with an aqueous stock solution of DMSA 0.3 mol × L^{-1} to obtain three magnetic fluid (MF) samples (DMSA-Mag), stably suspended in aqueous medium. The DMSA concentration used for surface coating the native nanosized maghemite (pMag sample) for further preparation of the magnetic suspensions was 0.025, 0.050, and 0.100 mol × L^{-1} whereas the three MF samples produced were labeled DMSA-Mag25, DMSA-Mag50, and DMSA-Mag100, respectively. The as-produced MF samples were shaken for 12 h and then dialyzed for 12 h against deionized water to eliminate the free DMSA from the bulk dispersion. The pH was adjusted to 7.0−7.2, and large aggregates were removed out from the MF sample by centrifugation at 5000 rpm, for 5 min. Though gel formation was observed for DMSA-Mag25, DMSA-Mag50 and DMSA-Mag100 revealed long-term colloidal stability. pDMSA-Mag25, pDMSA-Mag50, and pDMSA-Mag100 represent the powders obtained after drying the corresponding MF samples.

Sample Characterization. X-ray diffraction (XRD) spectra of the nanosized powder samples (magnetite and maghemite) were recorded in the range 19−80° (2θ) using a Shimadzu (XRD-6000) system equipped with the Cu Kα radiation source. The XRD data were refined using the PowderX software[31] and the cell parameters were calculated using the Unitcell software applied to the peak positions of all major reflections. The average diameter of the nanocrystalline domains was determined from the full-width at half-maximum (fwhm) of the strongest reflection peak (311 reflections) using the Scherrer's equation.[32] We found from the XRD data (not shown) that the average maghemite nanoparticle diameter was equals to 8 nm. The iron content was determined by atomic absorption spectrophotometry using a commercial Perkin-Elmer 5000 system. The stable MF samples (DMSA-Mag50 and DMSA-Mag100) presented concentration of about 10^{16} particle/mL, corresponding to about 0.4 mol × L^{-1} of Fe. Transmission electron microscopy (TEM) micrographs of the maghemite-based sample were recorded to assess the average particle size and size dispersion. Figure 1a shows a typical TEM micrograph of the DMSAMag100 sample, recorded in a JEOL 1011 transmission electron microscope. Vertical bars

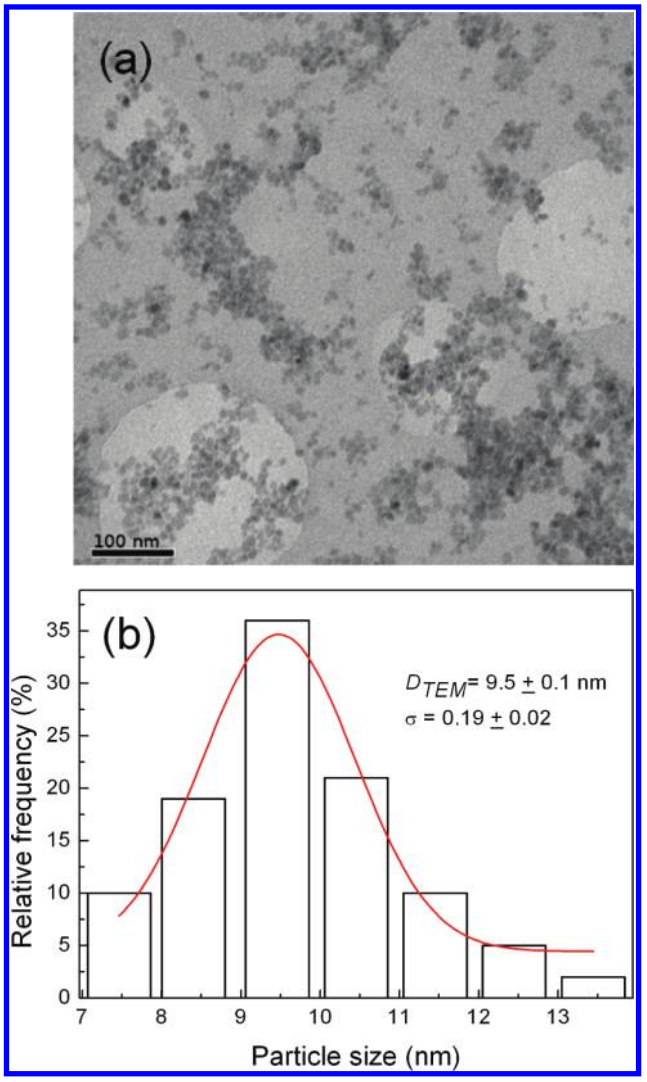

Figure 1. (a) TEM micrograph and (b) corresponding particle size histogram (vertical bars) of DMSA-Mag100 sample. The solid line represents the best curve-fitting using the log-normal distribution function.

in Figure 1b represent the particle size histogram obtained from the TEM micrographs whereas the solid line results from the curve-fitting of the data using the log-normal distribution function.[33] Values of the average particle diameter (D_{TEM}) and standard diameter deviation (σ) obtained from the fitting of the data presented in Figure 1b were 9.5 ± 0.1 nm and 0.19 ± 0.02, respectively. This average diameter is in close agreement with the crystallite size of the nanoparticles assessed by XRD.

The sulfur content of the prepared samples (DMSA-coated nanoparticles) was obtained from elemental analysis, and the average content of DMSA associated with the nanoparticles was estimated from both the average nanoparticle size (XRD data) and density of bulk maghemite. The measurement of sulfur content in the powder samples was performed using a Perkin-Elmer CHNS 2400. The sulfur content in pDMSA-Mag50 and pDMSA-Mag100 were 2.7×10^{-4} and 4.1×10^{-4} mol g^{-1}, respectively. From these results we estimate a total of 0.5 (pDMSA-Mag50) and 0.8 (pDMSA-Mag100) DMSA molecules grafted per nm^2 of maghemite. These values are equivalent to 105 (pDMSA-Mag50) and 160 (pDMSA-Mag100) DMSA molecules per particle, assuming no disulfide bridge formation. An estimation of the amount of ligand required to completely coat all the nanoparticle surface would be done considering the data for a similar nanoparticle surface-coated with oleic acid. In the case of the oleic acid molecule, with a net surface of 0.2 nm^2, the maximum oleic acid-grafting onto the surface of a 8.0 nm diameter nanoparticle should be around 1000.[24] Considering that DMSA molecules have two carboxylate terminals, the amount necessary to completely cover the nanoparticle surface would be between 500 and 1000 DMSA molecules. As mentioned, the DMSA-grafting achieved in this study (105−160 DMSA molecules per particle) is well below the value required to completely cover the nanoparticle surface.

The hydrodynamic diameters were measured by photon correlation spectroscopy (PCS) using the Zeta Plus equipment from Brookhaven Instruments Corp. The observed hydrodynamic diameters were 130 and 77 nm for DMSA-Mag50 and DMSA-Mag100, respectively. Taking into account the maghemite core sizes, these hydrodynamic values reveal no individual surface-functionalized particles, more likely clusters of particles instead, as will be discussed latter in this paper. The Raman system used to record the spectra is a commercial triple spectrometer (Jobin Yvon Model T64000) equipped with a CCD detector. The 514 nm line from an argon ion laser was used to illuminate the samples and all Raman data were recorded at room temperature. The PAS experimental setup consists of a sample enclosed in a sealed cell at atmospheric pressure coupled to a sensitive microphone. A $^1/_2$ in. condenser microphone (Bruel and Kjær, model 3547) was used to monitor the pressure change within the cell. A 150 W Xe lamp coupled to a 0.22 m double monochromator (Spex model 1680) was used as the variable wavelength light source. The light was chopped at a frequency of a few hertz, and the signal was processed by a lock-in amplifier (Stanford Research SR830). All the PA spectra were normalized to the spectra of a highly absorbing (black) film recorded in the same wavelength range.

RESULTS AND DISCUSSION

Considering the maghemite core size obtained, the hydrodynamic values we found for DMSA-Mag50 and DMSA-Mag100, respectively equal to 130 and 77 nm, indicate the presence of small clusters consisting of a few nanoparticles, more likely with the S−S bridge formation playing a central role in the particles' agglomeration process. Notice that the hydrodynamic diameter of the suspended units reduces as DMSA surface-functionalization increases. This finding strongly suggests the presence of two competitive S−S bridging mechanisms. The first one involves S−S bridge formation from neighboring DMSA-functionalized particles, hereinafter named interparticle S−S bridging, dominating the system's behavior at the lower surface functionalization content. The second one involves S−S bridge formation from neighboring DMSA molecules attached to the same nanoparticle surface, hereinafter named intraparticle S−S bridging, dominating the system's behavior at the higher surface functionalization content. At lower DMSA surface functionalization the free S−H groups from neighboring grafted molecules are far apart at the nanoparticle's surface making the interparticle S−S bridging more favorable, leading to sample gelification, as observed in the case of DMSA-Mag25. In contrast, at higher DMSA surface functionalization the free S−H groups from neighboring grafted molecules are closer together, making the

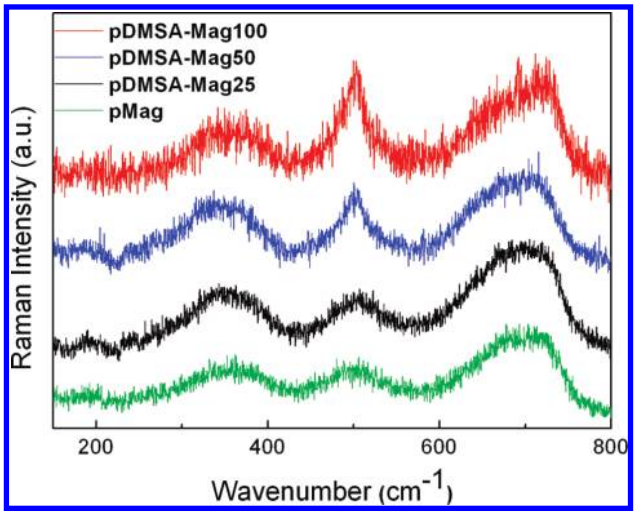

Figure 2. Raman spectra recorded for pMag, pDMSA-Mag25, pDMSA-Mag50, and pDMSA-Mag100 using the 514 nm laser line.

intraparticle S−S bridging the dominant mechanism, avoiding particle agglomeration and leading to higher colloidal stability, as observed in the case of DMSA-Mag100. As the DMSA grafting content increases, particle agglomeration decreases, leading to lower values of hydrodynamic diameters, as observed while evaluating DMSA-Mag25, DMSA-Mag50, and DMSA-Mag100. To the best of our knowledge the two proposed S−S bridging scenarios has not yet been mentioned in the literature, though it provides the explanation for the observed colloidal stability of the DMSA-grafted nanosized particles.

Figure 2 displays the Raman spectra of pMag, pDMSA-Mag25, pDMSA-Mag50, and pDMSA-Mag100, recorded under 0.2 mW optical excitation intensity. As already reported in the literature, no maghemite to hematite transformation was observed in all samples investigated under the optical excitation intensity employed in the present study (0.2 mW).[34,35] In the spectral region from 150 to 800 cm^{-1} the Raman features of the surface-uncoated nanosized maghemite (pMag) have been assigned to vibrational modes associated to the γ-Fe_2O_3 crystal structure.[24] Our spectra fitting procedure of pMag, using Lorentzian-like components, showed the presence of four structures: three of them at 352 (E_g), 503 (T_{2g}), and 673 cm^{-1} (A_{1g}), attributed to modes associated to tetrahedral iron sites, and the fourth one peaking at 721 cm^{-1} and assigned to octahedral iron sites.[36] The Raman spectra of DMSA-grafted samples, however, revealed a new sharp feature peaking at 500 cm^{-1}. Furthermore, the intensity of the Raman feature peaking at 500 cm^{-1} increases as the nominal concentration of the DMSA solution used to functionalize the pMag sample increases. According to the literature, the Raman feature at 500 cm^{-1} was assigned to the S−S stretching vibration[37,38] and represents the difference regarding the spectra of DMSA-grafted in comparison with the surface-uncoated sample (pMag). Note that the characteristic S−H Raman feature of DMSA,[39] expected to be found at 2566 cm^{-1}, was not observed in pDMSA-Mag25, pDMSA-Mag50, and pDMSA-Mag100. Therefore, the presence of the Raman band assigned to S−S bridges in the spectra of DMSA-grafted samples, we hypothesize, is due to the oxidation of neighboring S−H groups into S−S bridges and related to the DMSA molecules attached onto the nanoparticle's surface. Furthermore, assuming that the S−S bridge formation takes place at the surface of the DMSA-SPIO system, a reduced number of S−H groups is expected to be left over at the heavily surface-functionalized maghemite. In addition, the number of available S−H groups reduces as the nominal DMSA concentration used in the surface functionalization process increases. This finding, namely the S−S bridge formation involving neighboring DMSA molecules grafted onto nanosized particles, has already been reported in the literature.[12,17,19,40] Nevertheless, to the best of our knowledge, the S−S bridge formation while reducing the available S−H groups has not yet been quantitatively reported in the literature. As far as the S−S bridge formation is concerned, the area under the Raman feature peaking at 500 cm^{-1} was evaluated as a function of the nominal concentration (0.025, 0.050, and 0.100 mol × L^{-1}) of the DMSA solution used to functionalize the pMag sample. These area values (Raman feature peaking at 500 cm^{-1}) we claim scale linearly with the S−S bridge content at the nanoparticle's surface and were normalized with respect to the value obtained for the pDMSA-Mag100 sample. The normalized Raman area values were quoted as N_R. Therefore, the content of the available S−H groups scales linearly with $(1 - N_R)$.

Figure 3 shows the PA spectra of pDMSA-Mag25, pDMSA-Mag50, and pDMSA-Mag100, recorded at room temperature and in the wavelength range 0.3−1.0 μm. For reference, the room-temperature PA spectra of pMag is included in the inset of Figure 3. As previously discussed in the literature,[25−27] the PA data shown in Figure 3 can be analyzed in terms of three distinct bands (band C, band S, and band L) in the wavelength range of our investigation (0.3−1.0 μm). Band C, related to the absorption of the incident light by the core nanoparticle, has been observed in the range 0.3−0.4 μm in SPIO-based biocompatible MF samples. Band S and band L are related to the molecular shell around the core nanoparticle. The PA band S is related to the hydrochalcogenide (−XH) layer built up around the ferrite-based nanoparticle surface and has been observed close to 0.50 μm. It has been reported that the band S intensity reduces as the amount of the −XH moiety is reduced at the nanoparticle surface.[41] Finally, in the 0.65−0.90 μm region, one usually observes a complex structure associated to band L, representing the PA signature of the chemical species used to surface-functionalize the nanoparticle. It is observed in Figure 3 that PA spectra in the band L region show different features in the three samples investigated, thus explaining the different content of DMSA molecules attached onto the maghemite surface. The details revealed in the band L region (see Figure 3), from one sample to another, indicate the differences in DMSA-grafted organization while ranging from interparticle up to intraparticle S−S bridging. In the present study we focused our attention on the PA intensity related to the band S. More specifically, the PA spectra shown in Figure 3 have been integrated in the range 0.42−0.65 μm (see spectral region between vertical dashed lines) to cover the typical PA response range associated with the hydrochalcogenide moiety. It was observed that the integrated PA signal we evaluated decreases as the nominal concentration (0.025, 0.050, and 0.100 mol × L^{-1}) of the DMSA solution used to functionalize the pMag sample increases. The integrated PA signals of pDMSA-Mag25, pDMSA-Mag50, and pDMSA-Mag100 were normalized with respect to the highest PA signal value we obtained, namely the integrated PA signal of pDMSA-Mag25. We claim that the normalized integrated PA signal we obtained scales linearly with the hydrochalcogenide (−XH) content at the nanoparticle surface. The normalized

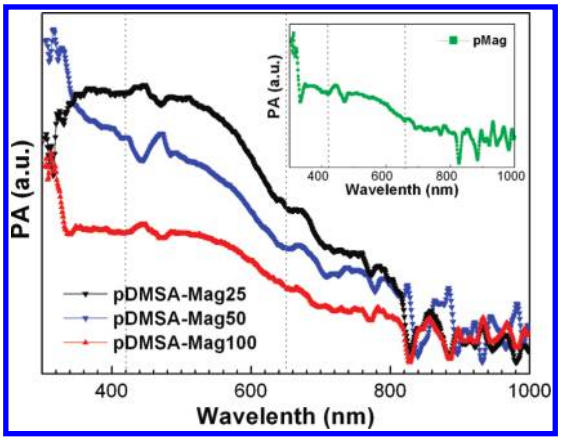

Figure 3. Photoacoustic spectra recorded for pDMSA-Mag25, pDMSA-Mag50, and pDMSA-Mag100. The dashed lines are only guides to show the band-S region. The inset shows the PA spectrum of pMag.

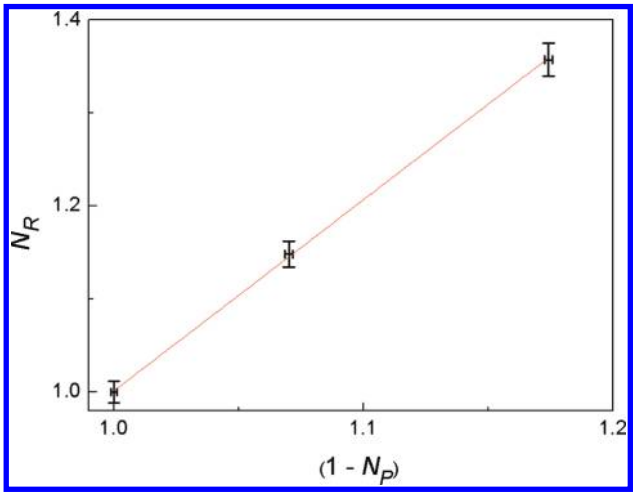

Figure 4. Normalized area values of the Raman feature peaking at 500 cm^{-1} (N_R) versus $(1 - N_P)$, where N_P values are the normalized integrated photoacoustic signal in the range 0.42−0.65 μm. The straight line across the experimental points is only a guide to the eyes.

integrated PA signal values were quoted as N_P. Therefore, the S−S bridge content at the nanoparticle surface scales linearly with $(1 - N_P)$.

Figure 4 shows the N_R versus $(1 - N_P)$ plot. Note the perfect linearity obtained from the data recorded using different experimental technique (Raman versus photoacoustic) while keeping small error bars. It is possible to infer from the data shown in Figure 4 that the absolute number of available S−H groups on DMSA-functionalized nanoparticles decreases as the nominal DMSA concentration increases. The observed linearity in Figure 4 represents the robustness and usefulness of both experimental techniques while probing the S−S bridge and the available S−H groups on DMSA-functionalized nanoparticles. This finding supports the use of both experimental techniques to quantitatively probe the presence of the above-mentioned moieties. Particularly interesting is the use of the PAS in quantitatively probe both the S−S and S−H moieties as a simple and inexpensive experimental technique. Notice that the photoacoustic effect has been successfully used in quality control[42−44] while correlation between the data taken from photoacoustic spectroscopy and well-established analytical techniques has been extensively reported in the literature.[45−47]

It is worth mentioning the linear relationship observed in the data displayed in Figure 4, despite the differences among the two spectroscopic techniques (RS and PAS). This finding strength the nondestructive analytical approach proposed in this study for probing thiol- and disulfide-containing moieties attached to the surface of nanosized materials. This is of great interest as S−H and S−S moieties appear in many biological molecules and play key roles in a variety of biochemical processes.

CONCLUSIONS

In conclusion, we found that relative quantification of the S−S bridge associated with DMSA molecules grafted onto nanosized maghemite particles (quoted as N_R) can be obtained using Raman spectroscopy. Correspondingly, we found that relative quantification of the S−H moiety associated with DMSA molecules grafted onto nanosized particles (quoted as N_P) can be accomplished using photoacoustic spectroscopy. As we hypothesize that S−S bridges are obtained from oxidation of neighboring S−H groups as the DMSA grafting coefficient increases toward saturation, the perfect linear relationship we find while plotting N_R versus $(1 - N_P)$ strongly supports this model picture. In addition, the analysis employed in the present report and the linear relationship presented in Figure 4 allows quantification of the [S−H]/[S−S] ratio in a wide range of DMSA-grafting values. Finally, the reduction of the hydrodynamic diameter of the colloidally suspended units as the DMSA surface grafting increases points out to two distinct S−S bridge formations: the intraparticle and the interparticle bridging, the latter leading to sample gelification (pDMSA-Mag25) and the former assuring good colloidal stability (pDMSA-Mag100). These findings are extremely important while modulating the attachment of biologically active molecules using the available S−H groups from DMSA-grafted nanoparticles.

AUTHOR INFORMATION

Corresponding Author

*Tel: +55-61-3307-2900. Fax: +55-61-3307-2363. E-mail: soler@unb.br.

ACKNOWLEDGMENT

The financial support from the Brazilian agencies MCT/CNPq, FAP-DF, FINEP, CAPES, and FUNAPE are gratefully acknowledged.

REFERENCES

(1) Viali, W. R.; Alcantara, G. B.; Sartoratto, P. P. C.; Soler, M. A. G.; Mosiniewicz-Szablewska, E.; Andrzejewski, B.; Morais, P. C. *J. Phys. Chem. C* **2010**, *114*, 179.

(2) Ross, R. W.; Zietman, A. L.; Xie, W.; Coen, J. J.; Douglas, M.; Dahl, J. M.; Shipley, W. U.; Kaufman, D. S.; Islam, T.; Guimaraes, A. R.; Weissleder, R.; Harisinghani, M. *Clin. Imag.* **2009**, *33*, 301.

(3) Leuschner, C.; Kumar, C. S. S. R.; Hansel, W.; Soboyejo, W.; Zhou, J.; Hormes, J. *Breast Cancer Res. Tr.* **2006**, *99*, 163.

(4) Alexiou, C.; Jurgons, R.; Schmid, R.; Hilpert, A.; Bergemann, C.; Parak, F.; Iro, H. *J. Magn. Magn. Mater.* **2005**, *293*, 389.

(5) Lin, M. M.; Kim, H.-H.; Kim, H.; Dobson, J.; Kim, D. K. *Nanomedicine* **2010**, *5*, 109.

(6) Pankhurst, Q. A.; Thanh, N. K. T.; Jones, S. K.; Dobson, J. *J. Phys. D: Appl. Phys.* **2009**, *42*, 224001.
(7) Mejias, R.; Perez-Yague, S.; Roca, A. G.; Perez, N.; Villanueva, A.; Canete, M.; Manes, S.; Ruiz-Cabello, J.; Benito, M.; Labarta, A.; Batlle, X.; Veintemillas-Verdaguer, S.; Morales, M. P.; Barber, D. F.; Serna, C. J. *Nanomedicine* **2010**, *5*, 397.
(8) Gupta, A. K.; Naregalkar, R. R.; Vaidya, V. D.; Gupta, M. *Nanomedicine* **2007**, *2*, 23.
(9) Tedesco, A. C.; Oliveira, D. M.; Lacava, Z. G. M.; Azevedo, R. B.; Lima, E. C. D.; Morais, P. C. *J. Appl. Phys.* **2003**, *93*, 6704.
(10) Corot, C.; Robert, P.; Idee, J.-M.; Port, M. *Adv. Drug Delivery Rev.* **2006**, *58*, 1471.
(11) Freitas, E. R. L.; Soares, P. R. O.; Santos, R. P.; Santos, R. L.; Silva, J. R.; Porfirio, E. P.; Báo, S. N.; Lima, E. C. D.; Guillo, L. A.; Morais, P. C. *J. Nanosci. Nanotechnol.* **2008**, *8*, 2385.
(12) Fauconnier, N.; Pons, J. N.; Roger, J.; Bée, A. *J. Colloid Interface Sci.* **1997**, *194*, 427.
(13) Chaves, S. B.; Lacava, L. M.; Lacava, Z. G. M.; Silva, O.; Pelegrini, F.; Buske, N.; Gansau, C.; Morais, P. C.; Azevedo, R. B. *IEEE Trans. Magn.* **2002**, *38*, 3231.
(14) Garcia, M. P.; Parca, R. M.; Chaves, S. B.; Silva, L. P.; Santos, A. D.; Lacava, Z. G. M.; Morais, P. C.; Azevedo, R. B. *J. Magn. Magn. Mater.* **2005**, *293*, 277.
(15) Valois, C. R. A.; Nunes, E. S.; Jaeger, R. G.; Lima, E. C. D.; Morais, P. C.; Azevedo, R. B. *J. Nanosci. Nanotechnol.* **2009**, *9*, 2846.
(16) Valois, C. R. A.; Braz, J. M.; Nunes, E. S.; Vinolo, M. A. R.; Lima, E. C. D.; Curi, R.; Kuebler, W. M.; Azevedo, R. B. *Biomaterials* **2010**, *31*, 366.
(17) Jun, Y.-W.; Huh, Y.-M.; Choi, J. S.; Lee, J.-H; Song, H.-T.; Kim, S.; Yoon, S.; Kim, K.-S.; Shin, J.-S.; Suh, J.-S.; Cheon, J. *J. Am. Chem. Soc.* **2005**, *127*, 5732.
(18) Huh, Y.-M.; Jun, Y.-W.; Song, H.-T.; Kim, S.; Choi, J.-S; Lee, J.-H.; Yoon, S.; Kim, K.-S.; Shin, J.-S.; Suh, J.-S.; Cheon, J. *J. Am. Chem. Soc.* **2005**, *127*, 12387.
(19) Chen, Z. P.; Zhang, Y.; Zhang, S.; Xia, J. G.; Liu, J. W.; Xu, K.; Gu, N. *Colloid Surf. A: Physicochem. Eng. Aspects* **2008**, *316*, 210.
(20) Bellamy, L. J. *The Infrared Spectra of Complex Molecules*, 3rd ed.; Chapman and Hall: London, 1975; pp 394−407.
(21) Möller, K.; Kobler, J.; Bein, T. *J. Mater. Chem.* **2007**, *17*, 624.
(22) Vargas, H.; Miranda, L. C. M. *Phys. Rep.* **1988**, *161*, 43.
(23) Morais, P. C.; da Silva, S. W.; Soler, M. A. G.; Buske, N. *J. Phys. Chem. A* **2000**, *104*, 2894.
(24) Soler, M. A. G.; Alcantara, G. B.; Soares, F. Q.; Viali, W. R.; Sartoratto, P. P. C.; Fernandez, J. R. L.; da Silva, S. W.; Garg, V. K.; Oliveira, A. C.; Morais, P. C. *Surf. Sci.* **2007**, *601*, 3921.
(25) Oliveira, A. C.; Tronconi, A. L.; Buske, N.; Morais, P. C. *J. Magn. Magn. Mater.* **2002**, *252*, 56.
(26) Avelino, S. R.; Oliveira, F. M. L.; Oliveira, A. C.; Morais, P. C. *J. Non-Cryst. Sol.* **2006**, *352*, 3692.
(27) Morais, P. C. *J. Alloys Compd.* **2009**, *483*, 544.
(28) Morais, P. C.; Santos, R. L.; Pimenta, A. C. M.; Azevedo, R. B.; Lima, E. C. D. *Thin Solid Films* **2006**, *515*, 266.
(29) van Ewijk, G. A.; Vroege, G. J.; Philipse, A. P. *J. Magn. Magn. Mater.* **1999**, *201*, 31.
(30) Rebodos, R. L.; Vikesland, P. J. *Langmuir* **2010**, *26*, 16745.
(31) Dong., C.; Chen, H.; Wu, F. *J. Appl. Crystallogr.* **1999**, *32*, 168.
(32) Cullity, B. D. *Elements of X-ray Diffraction*; Addison Wesley: Reading, MA, 1978; p 101.
(33) Popplewell, J.; Sakhnini, L. *J. Magn. Magn. Mater.* **1995**, *149*, 72.
(34) da Silva, S. W.; Melo, T. F. O.; Soler, M. A. G.; Lima, E. C. D.; Da Silva, M. F.; Morais, P. C. *IEEE Trans. Magn.* **2003**, *39*, 2645.
(35) de Faria, D. L. A.; Venancio Silva, S.; de Oliveira, M. T. *J. Raman Spectrosc.* **1997**, *28*, 873.
(36) Jacintho, G. V. M.; Brolo, A. G.; Corio, P.; Suarez, P. A. Z.; Rubim, J. C. *J. Phys. Chem. C* **2009**, *113*, 7684.
(37) Okabayashi, H.; Izawa, K.; Yamamoto, T.; Masuda, H.; Nishio, E.; O'Connor, C. J. *Colloid Polym. Sci.* **2002**, *280*, 135.
(38) Murty, K. V. G. K.; Venkataramanan, M.; Pradeep, T. *Langmuir* **1998**, *14*, 5446.
(39) Li, N. B.; Niu, L. M.; Luo, H. Q. *Microchim. Acta* **2006**, *153*, 37.
(40) Roca, A. G.; Veintemillas-Verdaguer, S.; Port, M.; Robic, C.; Serna, C. J.; Morales, M. P. *J. Phys. Chem. B* **2009**, *113*, 7033.
(41) Morais, P. C.; Oliveira, A. C.; Tronconi, A. L.; Gansau, C.; Goetze, T.; Buske, N. *IEEE Trans. Magn.* **2003**, *39*, 2654.
(42) Favier, J. P.; Bicanic, D. *Anal. Chem.* **1996**, *68*, 729.
(43) Beck, H. A.; Bozoki, Z.; Niessner, R. *Anal. Chem.* **2000**, *72*, 2171.
(44) Doka, O.; Bicanic, D. *Anal. Chem.* **2002**, *74*, 2157.
(45) Saucy, D. A.; Simko, S. J.; Linton, L. W. *Anal. Chem.* **1985**, *57*, 871.
(46) Torres, R. A.; Palmer, C. E. A.; Baisden, P. A.; Russo, R. E.; Silva, R. J. *Anal. Chem.* **1990**, *62*, 298.
(47) Childers, J. W.; Rohl, R.; Palmer, R. A. *Anal. Chem.* **1986**, *58*, 2629.